

**Harvard-Smithsonian Center for Astrophysics**  
**Precision Astronomy Group**  
60 Garden St., M/S 63, Cambridge, MA 02138

Date: 2000 March 24

TM00-01

To: Distribution

From: J.F. Chandler and R.D. Reasenberg

Subject: FAME centration sensitivity to focal length

## I. INTRODUCTION

One of the important design parameters in the FAME mission is the focal length, which determines not only the size of the instrument, but also the angular size of its field of view as a whole and of the pixels on the detectors. This memorandum describes the results of a study of the sensitivity of image centering for two different aperture obscurations and three different focal lengths at three different star temperatures, representing the gamut of spectral types. On the basis of these results, we draw some conclusions about the FAME mission, primarily, that any of the three focal lengths examined would give acceptable position uncertainties. Further, since the (photon-counting) statistical uncertainty is roughly an order of magnitude smaller than the desired mission accuracy, it should not be a major factor in designing the instrument or mission.

## II. CONFIGURATION

As described in our previous memorandum (Chandler and Reasenberg 1999), we combine the many observations of a single star taken during a “visit” to obtain uncertainties for both the spectral parameters (temperature and magnitude, assumed constant within the visit) and the positions (pixel phases of the image center). We have followed the same procedures as before, but some of the parameters have changed. In particular, the number of observations analyzed together is no longer fixed at seven. (See below.) As always, we expect the star image position to be distributed randomly with respect to the pixel boundaries. However, rather than throw a Monte Carlo set of pixel phases to analyze, we continue to adopt a set of evenly spaced phases over the whole pixel, but offset from zero phase to avoid the special cases of minimum and maximum sensitivity. (The use of Monte Carlo phases would introduce an additional degree of freedom and would thus require that each covariance study be repeated several times to average over the effects of the random pixel phases.)

In addition, we have taken the expanded aperture size of  $0.6 \text{ m} \times 0.25 \text{ m}$ , and we are now varying the focal length, using not only the old and new values of 7.5 and 15 m, but also a shorter value 3.75 m for comparison. In this study, we have adopted new values also for the instrument’s optical throughput, namely, 63% for the detector quantum efficiency, and 98% for the mirror reflectivity (at each of 9 reflections).\* We

---

\* Although the reflectivity of 98% is the current best estimate, the issue of the stability

continue to assume four-color photometry with 1% uncertainties to be combined with astrometric measurements with uncertainties based on photon statistics.

As before, we can view a “single-measurement position precision” only indirectly, since no single measurement determines a position (plus star parameters) all by itself. For comparison purposes, we simply scale the batch composite position uncertainty (as defined at the end of Section III) by root-N. The number N of observations in a visit comes from a simple calculation using the fact that the precession rate is 0.5 deg per spacecraft rotation, independent of the spin rate, and the further fact that the plane-of-sky angular width of each CCD chip is inversely proportional to the focal length. With the nominal design consisting of 20 chips, each spanning 2048 pixels of 15  $\mu\text{m}$ , we get, respectively, 52, 26, and 13 observations expected per star per visit, for the focal lengths of 3.75, 7.5, and 15 m.

However, our judging criterion should be the precision of the mission as a whole, not of a single measurement. Consider, then, the total number of observations of each star. Assuming we hold fixed the time required for a star to cross a CCD, the rotation rate scales inversely with the focal length, and so does the precession rate. Thus, the number of visits in a given time interval does also. Therefore, increasing the focal length by a factor of two decreases the number of measurements per star by a factor of four.

All observations in this study are computed from the set of model stellar spectra supplied to us by R. L. Kurucz (1999) and based principally on his stellar models. See Lejeune et al. (1997, 1998) for a description of these model spectra. We are still using solar metallicity and main-sequence surface gravity in these simulations, even though we now have software for varying and estimating those parameters. (The estimation of those parameters will be addressed in a future study.) For this study, there are three fictitious stars, with temperatures chosen near the bottom, middle and top of the range covered by the Kurucz model, namely, 3750, 8750, and 28,000 K. All three stars have magnitude  $V = 9$ .

We have used two different values for  $\kappa$ , the aperture’s fractional central obscuration, thus producing two whole sets of results which are qualitatively similar. The two values are 0.4 and 0.2. In the following discussion, any generalizations should be interpreted as applying to both values of  $\kappa$ , except where we refer explicitly to one or the other.

### III. RESULTS

We have performed a sensitivity study for each of the three focal lengths, using each of the three fictitious stars. In each of the nine solutions, we combine the four-color photometry with the appropriate number of astrometric measurements for a single visit of a single star and estimate the star’s temperature and magnitude, as well as the position for each astrometric measurement. In this study, the measurements are computed from the same model used in the analysis and are uncorrupted by noise. Thus, the only interesting results are the parameter correlations and statistical

---

of the reflectivity has not yet been addressed. Should it be necessary to achieve stability by changing to a significantly lower reflectivity, say 85%, the net effect would be not quite doubling the statistical uncertainties.

uncertainties.

The correlations are all rather low, aside from the one between temperature and magnitude. (See Tables 1 and 2.) Between pairs of positions, the correlations are mostly less than 1%, though a few are as high as 5% for the 3.75 m focal length. The correlations between temperature and position depend on temperature and focal length. With  $\kappa = 0.4$  at 3.75 m, the correlations range up to 18% for the cool star (3750 K) and up to 31% for the hotter stars. With  $\kappa = 0.2$ , the corresponding limits are 10% and 21%, respectively. These correlations are all smaller for the longer focal lengths, just as the position-position correlations are. Figure 1 shows the most dramatic case (3.75 m, 28,000 K,  $\kappa = 0.4$ ). The plot has been reflected about the origin, taking advantage of the explicit odd symmetry in the model, to achieve a higher density of points and more clearly reveal the shape of the correlation function. This symmetry follows directly from the explicit symmetries of the partial derivatives of intensity with respect to temperature and pixel phase, respectively, even and odd. Figure 2 is the corresponding plot for  $\kappa = 0.2$ .

The graphs of position sensitivity versus pixel phase display wide variations with focal length and, to a lesser extent, with temperature. Figures 3, 4, and 5 show all nine of these graphs for  $\kappa = 0.4$ , while Figures 6, 7, and 8 show the graphs for  $\kappa = 0.2$ . These graphs have also been folded about the line of zero pixel phase (but with even symmetry). The basic characteristics of these plots are easily understood in terms of the relative widths of the pixels and the various peaks in the point spread functions (PSF). For a sufficiently short focal length, the central PSF peak can fit entirely within one or two pixels, leading to a maximum in sensitivity when the relevant pixel boundary falls exactly on the PSF peak. Conversely, if the pixel boundaries fall only on or near “nulls”, the sensitivity reaches a minimum. In Figures 9 and 10, we show central cross-sections along the scan direction of the PSF’s for the two values of  $\kappa$ . The two figures are superficially very similar, but differ in details such as the width of the central peak and the relative heights of the central and adjacent peaks. For example, the ratio of the peak heights (second peak divided by central peak) is 0.38 for  $\kappa = 0.4$ , while it is as low as 0.16 for  $\kappa = 0.2$ .

Although the sensitivity varies widely with pixel phase, there is a characteristic mean position uncertainty that comes from the combined analysis of the observations. In the limit where the instrument rotation is known perfectly, the observations of a star can be mapped onto a common frame of reference, and it is appropriate to estimate a single position for the star in that frame. Mathematically, that is equivalent to setting  $\phi = \phi_1 = \phi_2 \dots \phi_n$ , where  $\phi_i$  is the phase of the  $i$ th observation of the star in question. Computationally, one can easily convert the normal equations from the case of a single observation of each of the  $\phi_i$  to the case of  $n$  observations of  $\phi$ : the rows and columns corresponding to the  $\phi_i$  are all added together to produce a single row and column, thus producing a reduced matrix. The same reduction is applied to the vector part of the normal equations.

Because of the model symmetries, the terms between position and any spectral parameter (temperature and magnitude in this case) tend to add up to zero and leave us with a decoupled position equation. The resulting “batch composite position uncertainty” for the visit is simply the inverse square root of the sum of the elements of

**Table 1.** Mean position uncertainties and temperature-magnitude correlations for obscuration  $\kappa = 0.4$ 

F (m)	Mean position precision ( $\mu\text{as}$ )						Correlations (Temperature-Magnitude)		
	Per Observation			Mission Result (2.5 year)					
	T (K):	3750	8750	28000	3750	8750	28000	3750	8750
3.75	351	369	345	3.9	4.1	3.9	-0.9961	0.9983	0.9999+
7.50	275	274	254	6.1	6.1	5.7	-0.9868	0.9942	0.9999
15.00	158	205	199	7.1	9.2	9.0	-0.9623	0.9717	0.9997

the (purely diagonal) information sub-matrix for positions. (With real data, for which the distribution in pixel phase will not be uniform, the cross terms will not be so nearly zero as in these test cases. Nonetheless, this simple calculation provides a reasonable approximation of the statistical batch uncertainty. A rigorous derivation of this method can be provided for the interested reader.)

These uncertainties are shown in Tables 1 and 2, having been scaled by the appropriate root-N factors to “mean” single-observation and mission levels. In the Tables, the uncertainties are presented under the heading “Mean position precision,” signifying the component of the precision attributable to statistical uncertainty. As stated above, there are 52, 26, and 13 observations, respectively, in each visit for the focal lengths 3.75, 7.5, and 15 m. In the Tables, we assume there are 16,000, 4000, and 1000 total observations per star for these three cases, corresponding to a mission length of 2.5 years for each. We further assume that these observations are distributed uniformly in position angle, so that, effectively, half of the observations contribute in each of the two orthogonal directions of the reference system. (We neglect here the contribution of the much weaker cross-scan position measurements.) For the analysis of the whole mission, the standard five astrometric parameters would be estimated for each star (not just the position). Provided that the position estimates are referred to the mean epoch of the mission, the position uncertainties will not be degraded appreciably by estimating the proper motions and parallaxes.

#### IV. DISCUSSION

The first conclusion that can be drawn from the tables is that the mission statistical uncertainties are all acceptably low. Provided that the rotational history of the spacecraft can be determined to sufficient accuracy, each scenario achieves an uncertainty better than 10  $\mu\text{as}$  (not counting any systematic errors in the CCD detectors, etc).

**Table 2.** Mean position uncertainties and temperature-magnitude correlations for obscuration  $\kappa = 0.2$ 

F (m)	Mean position precision ( $\mu\text{s}$ )						Correlations (Temperature-Magnitude)		
	Per Observation			Mission Result (2.5 year)					
T (K):	3750	8750	28000	3750	8750	28000	3750	8750	28000
3.75	259	268	251	2.9	3.0	2.8	-0.9964	0.9983	0.9999+
7.50	194	193	179	4.3	4.3	4.0	-0.9906	0.9958	0.9999+
15.00	118	135	129	5.3	6.0	5.9	-0.9686	0.9815	0.9998

Second, we find confirmation of the expectation that increasing the focal length (and correspondingly increasing the number of pixels covered by a star image) improves the mean single-measurement position uncertainty. There is, of course, an associated cost in terms of increased requirements for data transmission per measurement, but the benefit is clear.

Third, we see that the overall mission precision is instead improved by decreasing the focal length. Although each measurement contributes less, the number of measurements more than compensates. Again, there is an associated cost (more measurements to transmit). In the absence of pixel co-adding, the two cost factors would cancel for the mission as a whole — the number of pixel counts per measurement and the number of measurements per star would go as the square and inverse-square, respectively, of the focal length. On the other hand, co-adding all the pixels in each row (i.e., in the cross-scan direction) would make the number of transmitted pixel counts per measurement rise only as the first power of focal length, thus making the net transmission cost favor longer focal lengths. In either case, this assumes that we select and send data only from the “interesting pixels” with no provision for the misplacement of the selection region on the CCD. Note that co-adding has not been included in this study; each solution here uses a two-dimensional array of pixels from each observation. Though we have not addressed co-adding in this study, we believe that co-adding in the transverse direction increases the scan-direction position uncertainty by only a little.

In all these conclusions, we have neglected the effect of CCD read noise, which becomes increasingly important for dimmer stars. For the three test stars in this study, with  $V = 9$ , the read noise is unimportant. Note that co-adding helps for faint stars for which read noise matters.

Another point not addressed by this study is the effect of changing the number of color bands in the photometry. This will be addressed in a future memorandum. In a limited fashion, we have considered the effect of leaving out the photometry altogether.

A few of the solutions reported in this study have been repeated without the 4-band photometry, and the resulting uncertainties are very nearly the same. (The advantage of having the four colors is in the speed of converging to a solution, rather than a significantly better result.)

## V. REFERENCES

- Chandler, J. F. and Reasenber, R. D., 1999, technical memorandum TM99-06 “FAME astrometry by centroiding analysis on multiple observations.”
- Kurucz, R. L. 1999, Private communication
- Lejeune, T., Cuisinier, F., & Buser, R., 1997, A&A Supp, 125, 229-246.
- Lejeune, T., Cuisinier, F., & Buser, R., 1998, A&A Supp, 130, 65-75.

## FIGURE CAPTIONS

**Figure 1.** The correlations between estimates of temperature and position as a function of pixel phase for a star of temperature 28,000 K, for a focal length of 3.75 m, using a central obscuration of  $\kappa = 0.4$ .

**Figure 2.** The correlations between estimates of temperature and position as a function of pixel phase for a star of temperature 28,000 K, for a focal length of 3.75 m, using a central obscuration of  $\kappa = 0.2$ .

**Figure 3.** The position uncertainties as a function of pixel phase, with an obscuration of  $\kappa = 0.4$ , for a star of temperature 3750 K for each of three possible focal lengths, plotted in arcsec.

**Figure 4.** The position uncertainties as a function of pixel phase, with an obscuration of  $\kappa = 0.4$ , for a star of temperature 8750 K for each of three possible focal lengths, plotted in arcsec.

**Figure 5.** The position uncertainties as a function of pixel phase, with an obscuration of  $\kappa = 0.4$ , for a star of temperature 28,000 K for each of three possible focal lengths, plotted in arcsec.

**Figure 6.** The position uncertainties as a function of pixel phase, with an obscuration of  $\kappa = 0.2$ , for a star of temperature 3750 K for each of three possible focal lengths, plotted in arcsec.

**Figure 7.** The position uncertainties as a function of pixel phase, with an obscuration of  $\kappa = 0.2$ , for a star of temperature 8750 K for each of three possible focal lengths, plotted in arcsec.

**Figure 8.** The position uncertainties as a function of pixel phase, with an obscuration of  $\kappa = 0.2$ , for a star of temperature 28,000 K for each of three possible focal lengths, plotted in arcsec.

**Figure 9.** The central cross-section through the PSF in the scan direction, with an obscuration of  $\kappa = 0.4$ , for a focal length of 15m. The same plot applies for the shorter focal lengths, but with the pixels scaled up correspondingly. In this plot, the second peak is 0.38 times as high as the central one.

**Figure 10.** The central cross-section through the PSF in the scan direction, with an obscuration of  $\kappa = 0.2$ , for a focal length of 15m. The same plot applies for the shorter focal lengths, but with the pixels scaled up correspondingly. In this plot, the second peak is 0.16 times as high as the central one.

DISTRIBUTION:

SAO:

R.W. Babcock      FAME web site via Marc Murison  
J.F. Chandler  
J.D. Phillips  
R.D. Reasenber  
I.I. Shapiro

Fig. 1: Position-temperature correlation for  $T=28000$ ,  $\kappa=.4$ ,  $F=3.75m$

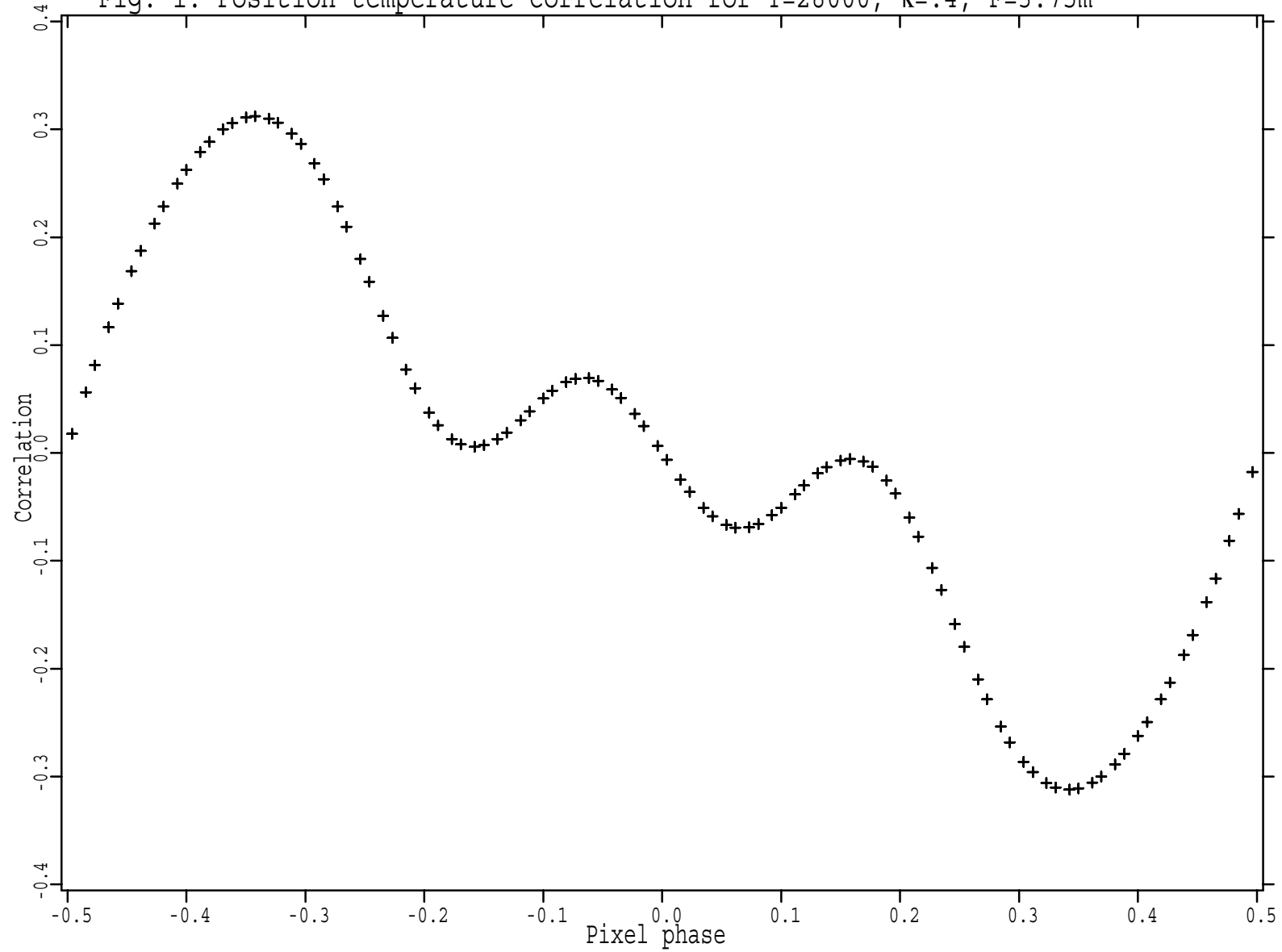


Fig. 2: Position-temperature correlation for  $T=28000$ ,  $\kappa=.2$ ,  $F=3.75m$

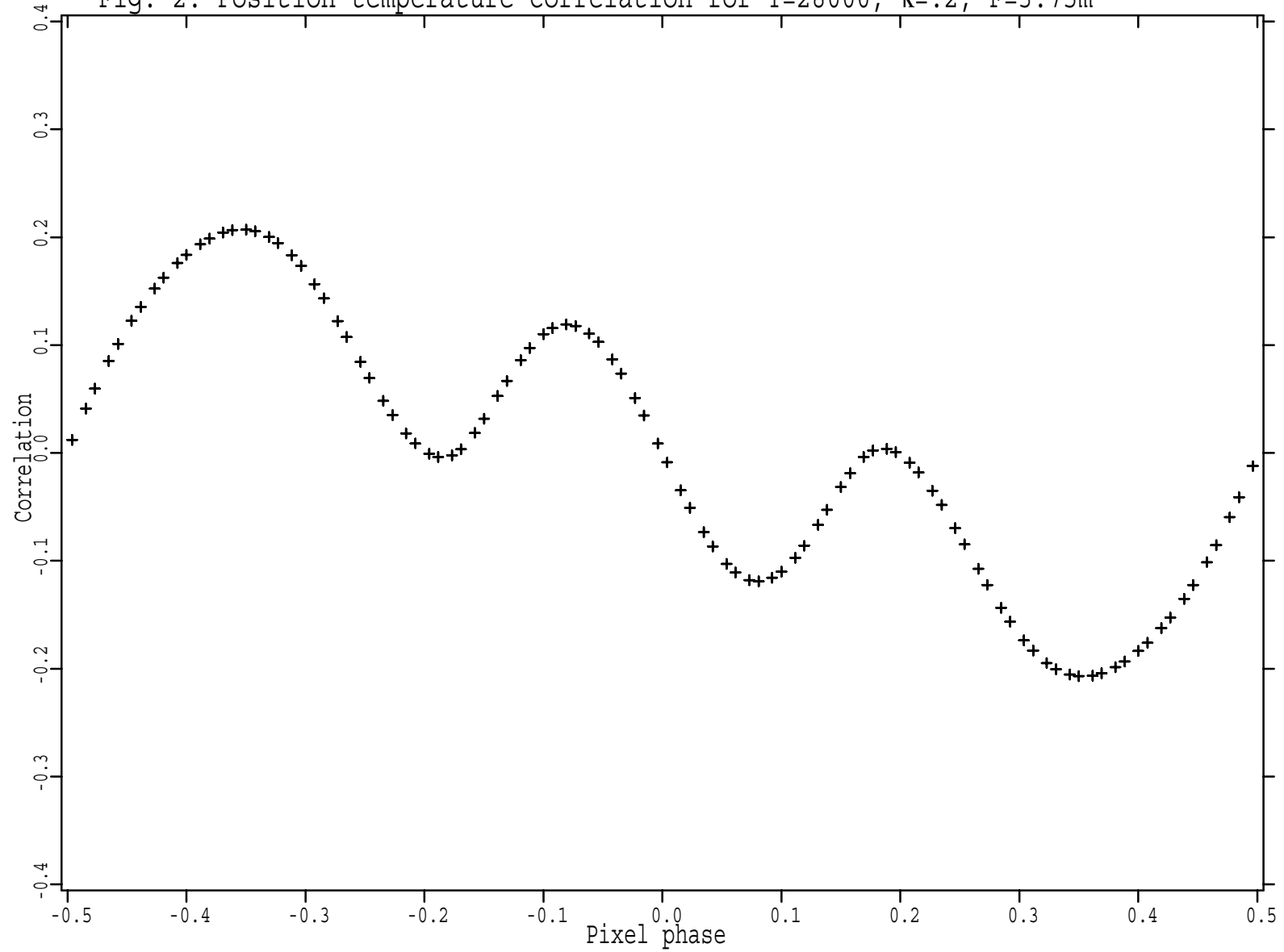


Fig. 3: Position sensitivity for  $T=3750$ ,  $\kappa=.4$ ,  $+,-,! = 3.75,7.5,15m$  F

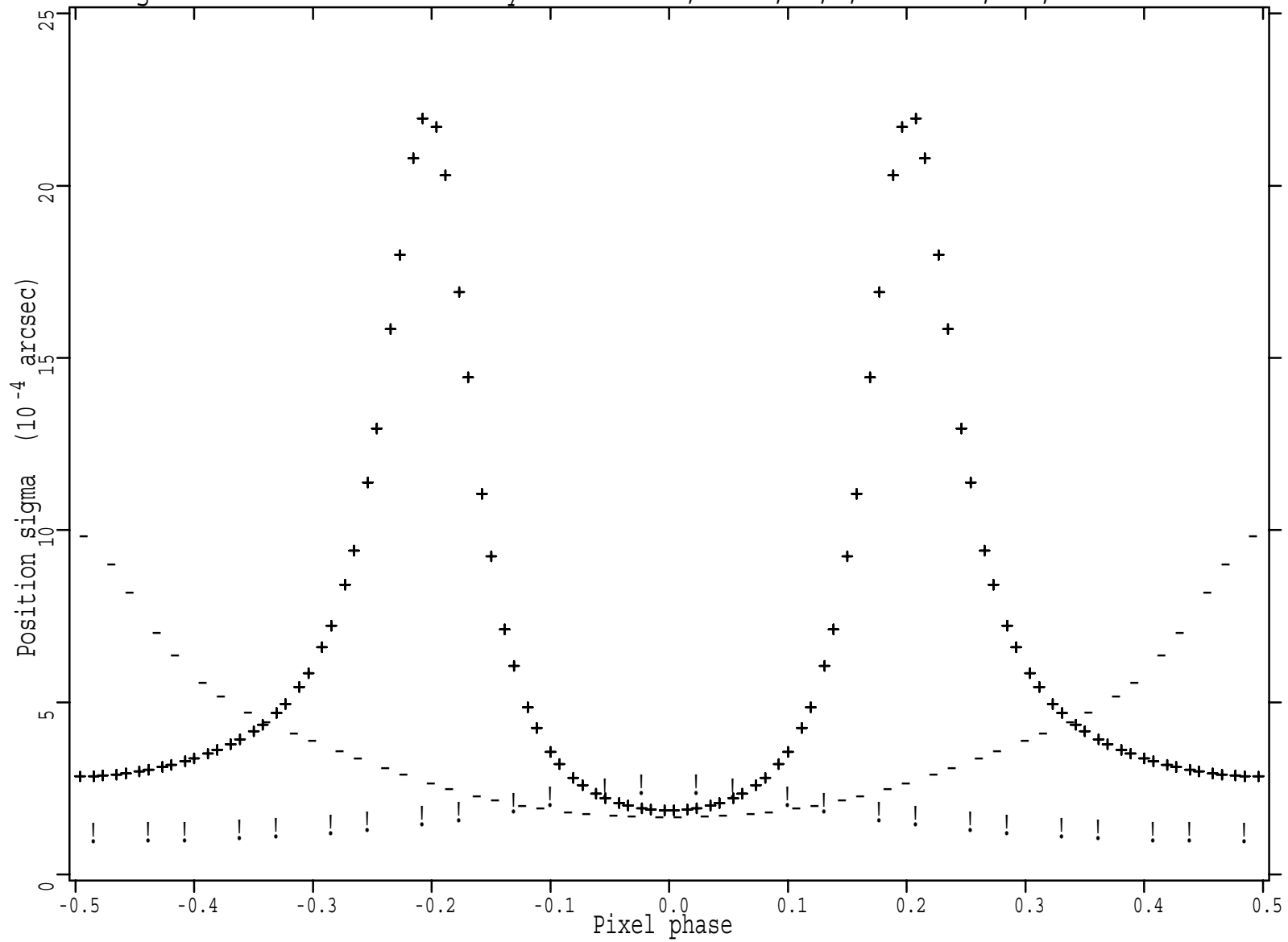


Fig. 4: Position sensitivity for  $T=8750$ ,  $\kappa=.4$ ,  $+,-,! = 3.75,7.5,15m$  F

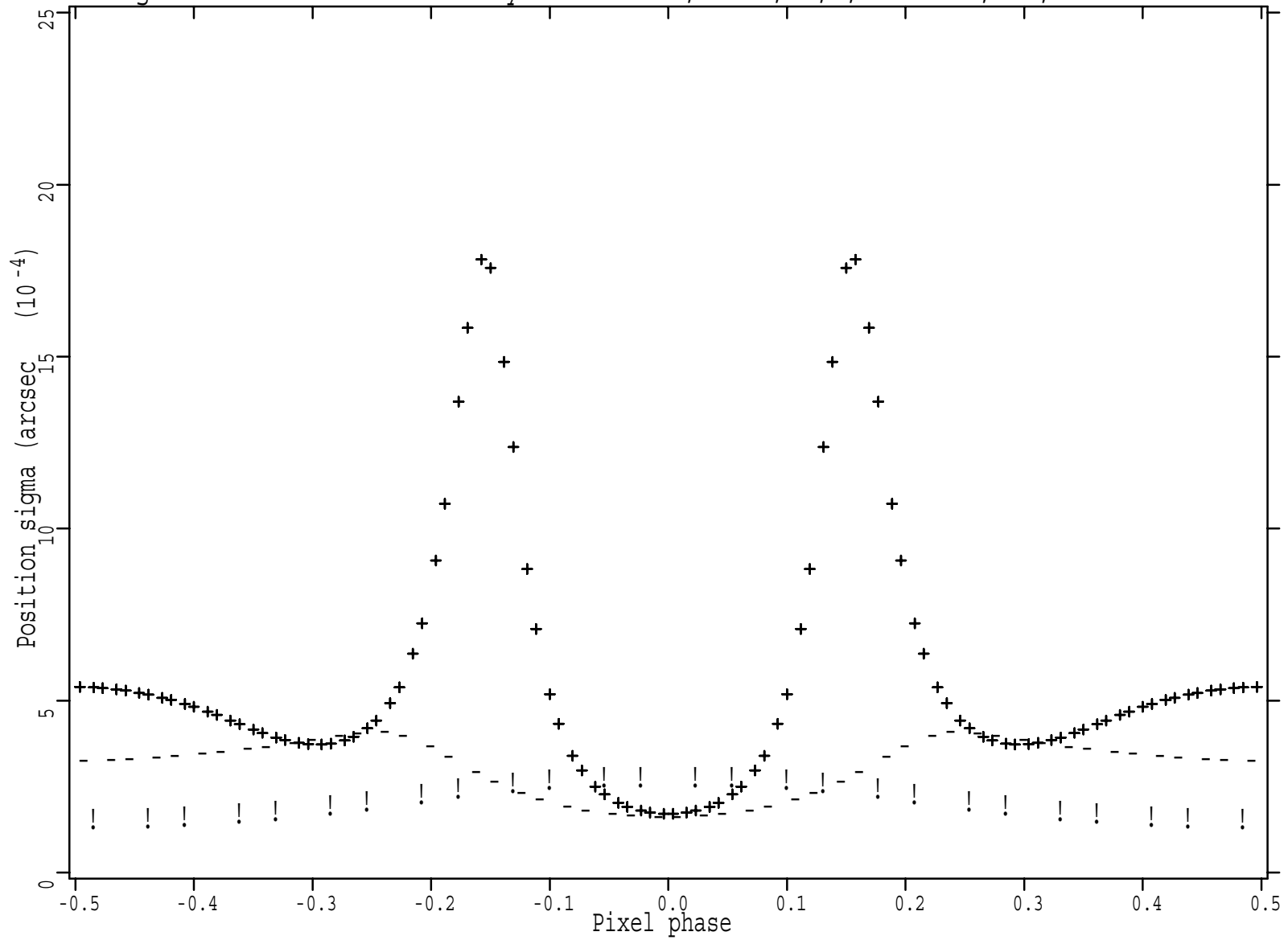


Fig. 5: Position sensitivity for  $T=28000$ ,  $\kappa=.4$ ,  $+, -, ! = 3.75, 7.5, 15m$  F

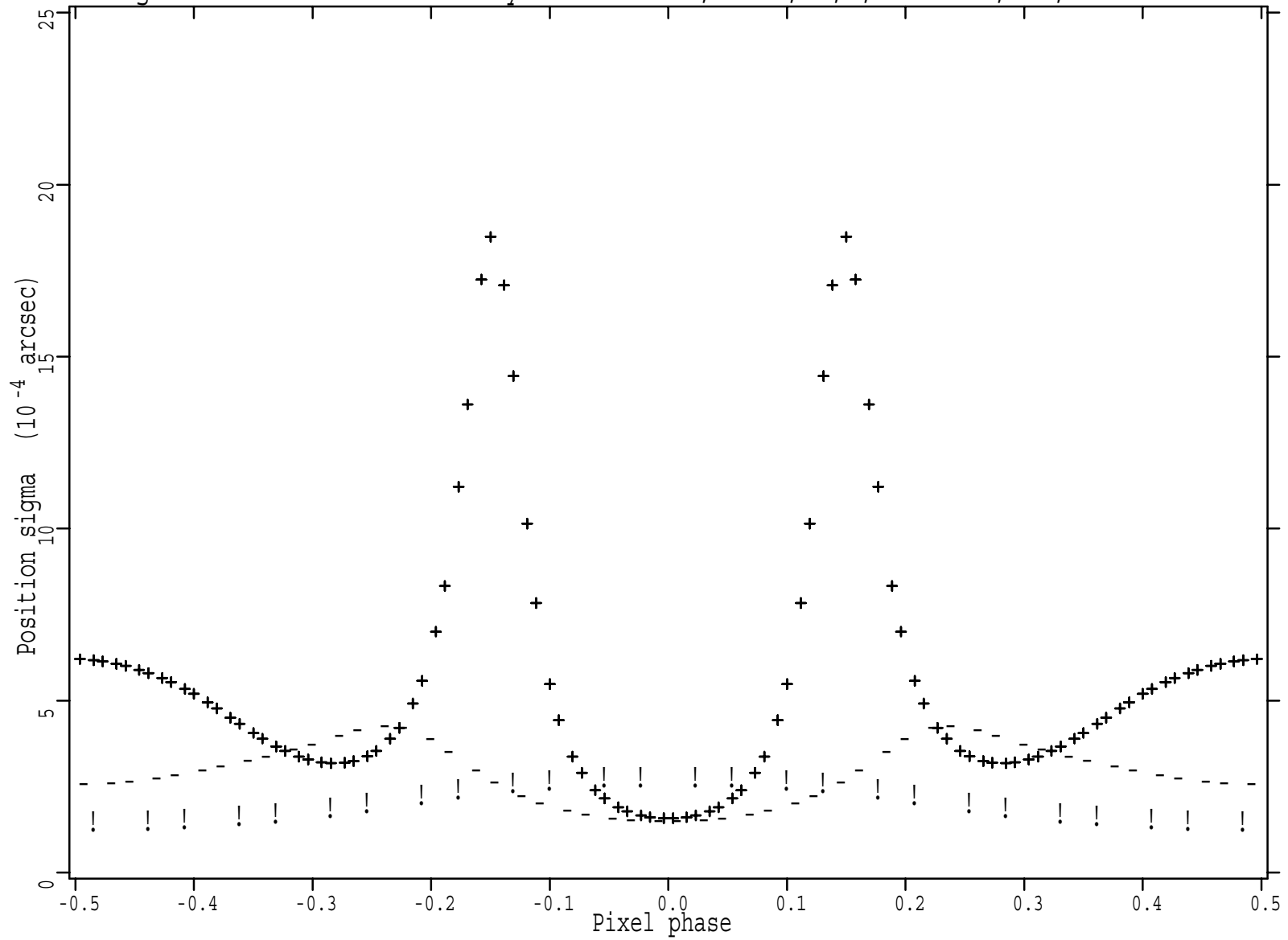


Fig. 6: Position sensitivity for  $T=3750$ ,  $\kappa=.2$ ,  $+,-,! = 3.75,7.5,15m$  F

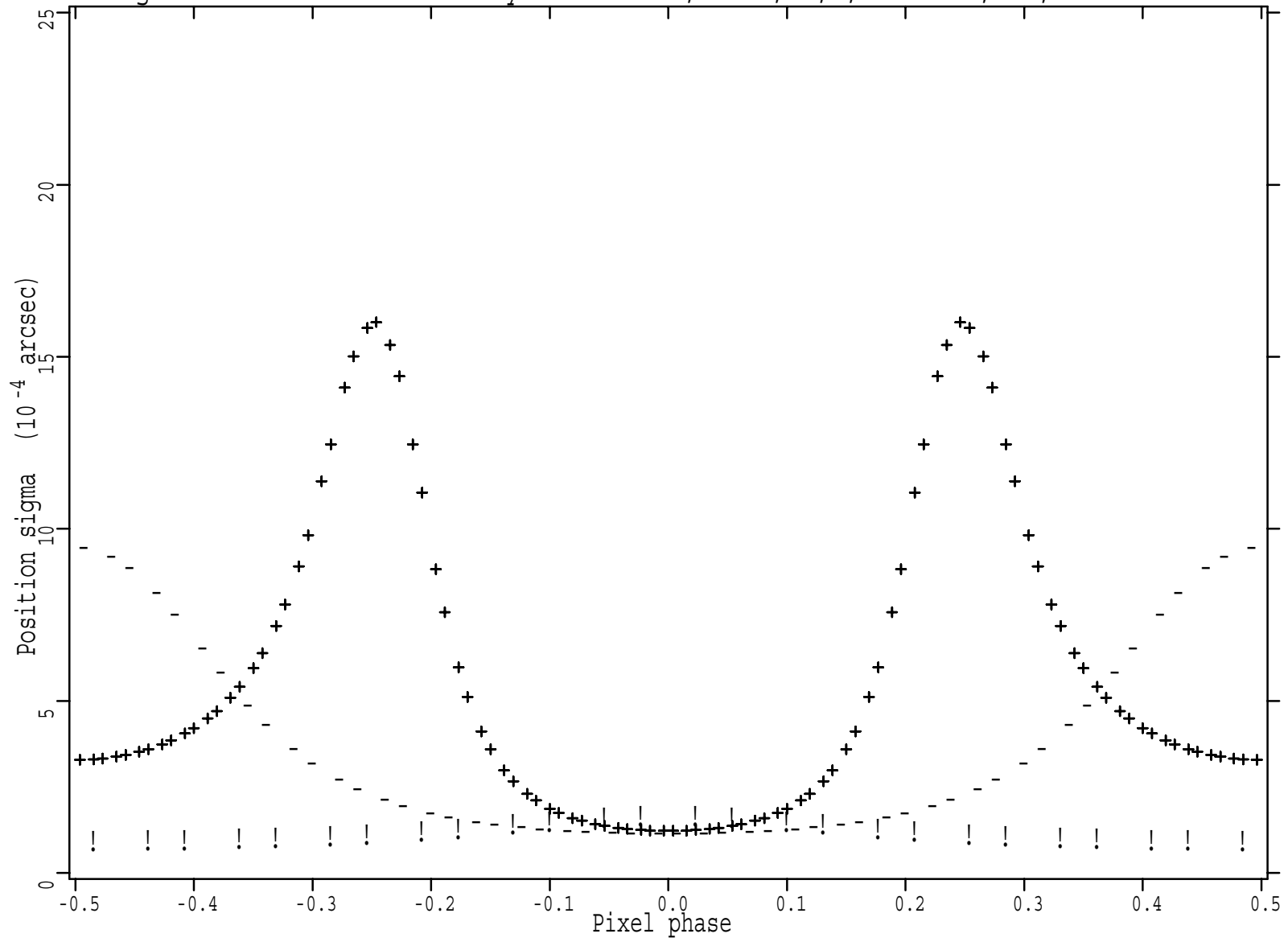


Fig. 7: Position sensitivity for  $T=8750$ ,  $\kappa=.2$ ,  $+,-,! = 3.75,7.5,15m$  F

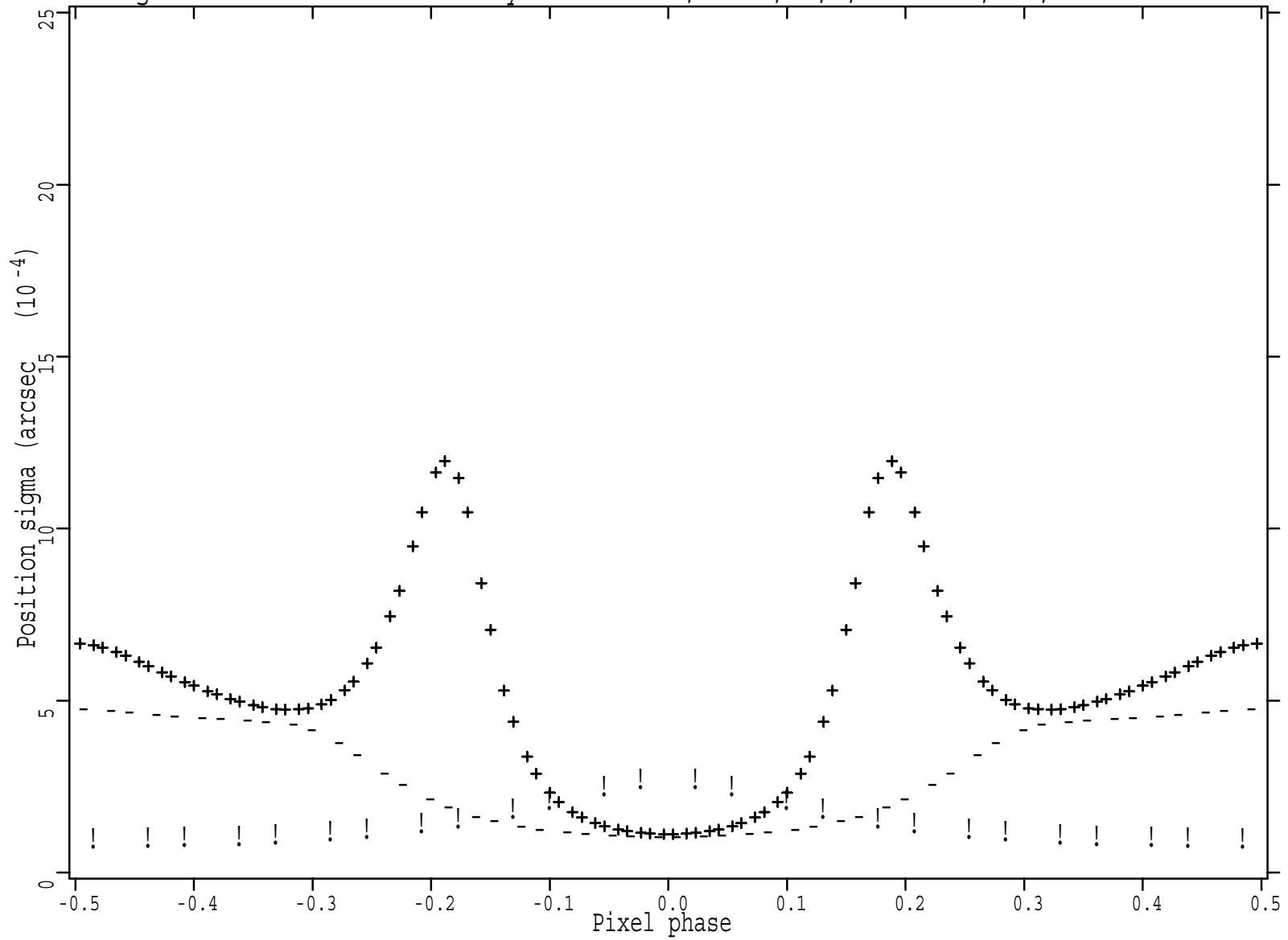


Fig. 8: Position sensitivity for  $T=28000$ ,  $\kappa=.2$ ,  $+, -, ! = 3.75, 7.5, 15m$  F

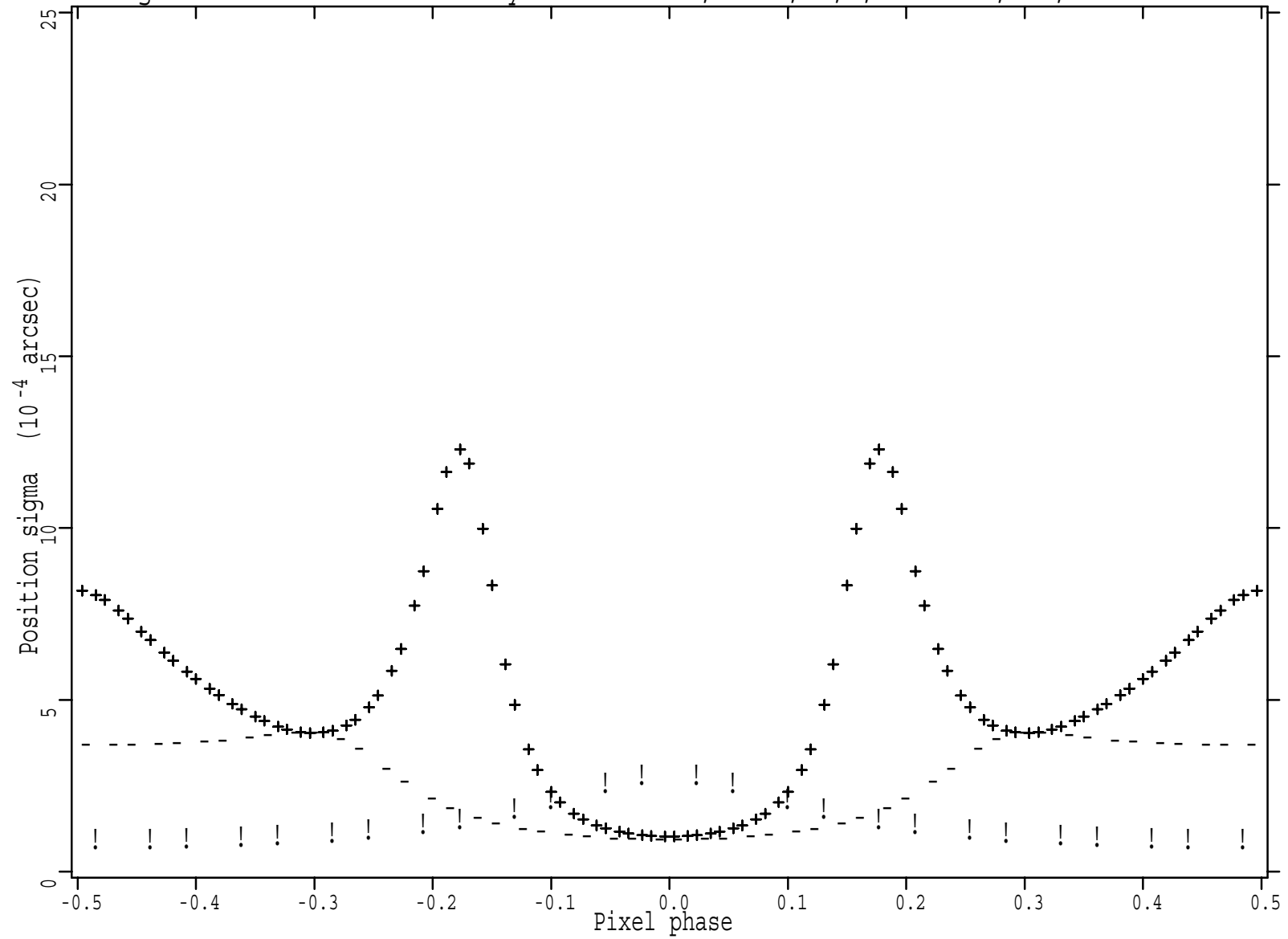


Fig. 9: PSF along scan direction,  $T=3750$  K,  $\kappa=.4$ ,  $F=15m$

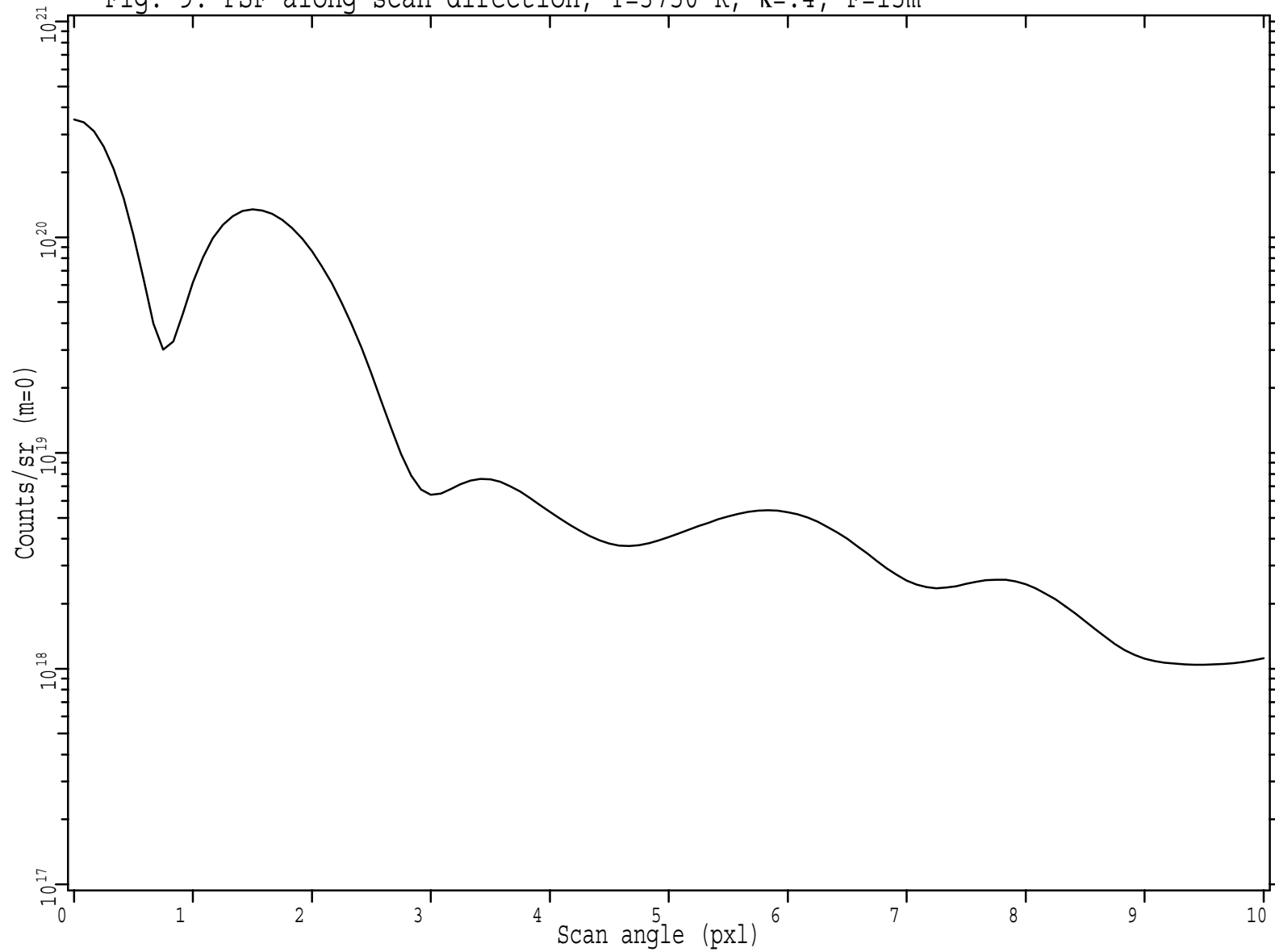


Fig. 10: PSF along scan direction,  $T=3750$  K,  $\kappa=.2$ ,  $F=15m$

